Gordon–Haus timing jitter in dispersion-managed systems with lumped amplification: analytical approach

C. J. McKinstrie*

Department of Mechanical Engineering, University of Rochester, Rochester, New York 14627

J. Santhanam

Department of Physics and Astronomy, University of Rochester, Rochester, New York 14627

Govind P. Agrawal

The Institute of Optics, University of Rochester, Rochester, New York 14627

Received April 26, 2001; revised manuscript received October 4, 2001

We use the moment method to calculate the Gordon–Haus timing jitter of optical pulses in dispersion-managed communication systems designed by use of lumped fiber amplifiers. The use of the Gaussian approximation for the chirped pulses, in combination with variational analysis, allows us to obtain an analytic expression for the timing jitter that is valid for an arbitrary number of amplifiers within each map period. We use this result to discuss how jitter is affected when more than one amplifier is used within each map period. We consider jitter for soliton-based systems as well as for low-power light-wave systems designed by use of the chirped return-to-zero format. In each case, the effects of dispersion compensation on the timing jitter are studied in detail. © 2002 Optical Society of America

OCIS codes: 060.2330, 190.5530, 060.4370, 060.5530.

1. INTRODUCTION

It has been known for many years that Gordon–Haus (GH) timing jitter imposes a fundamental limitation on long-haul soliton systems designed with amplifiers placed periodically along the fiber link.[1–6] Physically, timing jitter originates from spontaneous emission that is added to the pulse train during its amplification inside each amplifier. It was originally believed that this jitter occurs only when solitons are used, and perturbation theory developed for solitons was used to describe it.[5] The GH jitter of solitons has been analyzed in systems made with constant-dispersion fibers,[1] dispersion-decreasing fibers,[3] and dispersion-managed (DM) fiber links.[7,8]

Recently it was recognized that timing jitter can occur with any transmission format, including the non-return-to-zero, the chirped-return-to-zero (CRZ), and the DM soliton formats,[7] and it can be calculated by use of the well-known moment method.[9] In this paper we present a simplified form of the moment method and show that it can provide approximate analytic expressions for timing jitter under quite realistic conditions as long as each bit in the DM system can be approximated by a chirped Gaussian pulse. We apply this technique to obtain an analytic expression for timing jitter even when several amplifiers are present within each map period. We study the effects of precompensation and postcompensation on the timing jitter in DM light-wave systems for both low-power CRZ and soliton formats. We find that one can reduce the timing jitter significantly by choosing the precompensation and the postcompensation of residual dispersion judiciously.

The paper is organized as follows: In Section 2 we present the basic moment equations and show how the position and the frequency shifts acquired by an optical pulse within an amplifier evolve along the fiber link. In Section 3 we calculate the variances and the cross correlation of the position and the frequency shifts at each amplifier, assuming that the pulse is in the form of a chirped Gaussian pulse. In Section 4 we show how the two shifts grow along the fiber link as the pulse propagates from one amplifier to the next. Section 5 deals with the case of solitons for which the pulse propagates in a periodic fashion and acquires the same parameter values at each amplifier. This property permits us to obtain an analytic expression for the timing jitter even when more than one amplifier is used in each map period. In Section 6 we show how the use of postcompensation can reduce the GH timing jitter of solitons. Section 7 is devoted to the low-power CRZ system in which the pulse propagates in a quasi-linear fashion. We are able to obtain an analytic expression for the timing jitter even in this case. In Section 8 we consider how the jitter can be minimized along the entire link by use of a judicial combination of precompensation and postcompensation. The main results are summarized in Section 9.

2. MOMENT EQUATIONS

A typical DM system consists of a precompensation fiber followed by a periodic sequence of anomalous- and normal-dispersion fibers, and finally a postcompensation fiber. At least one amplifier is used per map period to

compensate for fiber losses. Each amplifier not only restores the pulse energy to its original input value but also adds noise through spontaneous emission. This noise perturbs each optical pulse such that its amplitude, width, position, chirp, frequency, and phase all vary in a random fashion along the fiber link. Amplitude fluctuations degrade the signal-to-noise ratio and affect system performance through a reduced value of the so-called Q parameter.[6] In contrast, frequency fluctuations affect the pulse position within the bit slot and introduce the GH timing jitter that also affects the system performance. In this paper we focus exclusively on the timing jitter issue.

Optical pulse propagation inside any kind of fiber is governed by the nonlinear Schrödinger equation[6]

$$i\frac{\partial U}{\partial z} - \frac{\beta_2}{2}\frac{\partial^2 U}{\partial t^2} + \gamma|U|^2U = -\frac{i\alpha}{2}U, \tag{1}$$

where U is the slowly varying amplitude of the pulse envelope, α accounts for fiber losses, β_2 is the group-velocity dispersion (GVD) coefficient, and γ is the nonlinear parameter that is responsible for self-phase modulation. For a DM system Eq. (1) cannot be solved analytically because the three parameters α, β_2, and γ are not constants but vary along the fiber link. Approximate solutions have been obtained with a variational technique for DM light-wave systems and were found through numerical simulations to be reasonably accurate.[10–14]

The use of numerical solutions for calculating GH timing jitter is quite time consuming because of the statistical nature of the problem. The moment method,[9] developed as early as 1971 for the study of self-focusing of laser beams, provides a short cut for evaluating timing jitter in DM systems.[7] In the moment method, one introduces pulse energy E, pulse position T, and frequency shift W (from the original carrier frequency) by using the formulas

$$E = \int_{-\infty}^{\infty}|U|^2\mathrm{d}t, \tag{2}$$

$$T = \frac{1}{E}\int_{-\infty}^{\infty}t|U|^2\mathrm{d}t, \tag{3}$$

$$W = \frac{i}{2E}\int_{-\infty}^{\infty}(U^*U_t - UU_t^*)\mathrm{d}t, \tag{4}$$

where the subscript t denotes a time derivative. One can use nonlinear Schrödinger equation to find how E, T, and W vary along the DM link. Differentiating Eqs. (2)–(4) with respect to z and using Eq. (1), we find that

$$\frac{\mathrm{d}E}{\mathrm{d}z} = -\alpha E, \qquad \frac{\mathrm{d}T}{\mathrm{d}z} = \beta_2 W, \qquad \frac{\mathrm{d}W}{\mathrm{d}z} = 0. \tag{5}$$

At each amplifier, E, T, and W change because of gain- and amplifier-induced noise. As we mentioned above, noise-induced changes in the pulse energy caused by intensity fluctuations are not considered in this paper. Thus, pulse energy E is a deterministic quantity that decreases as $\exp(-\alpha z)$ in each fiber section. By construction, amplifier gain compensates for all fiber losses that accumulate in the preceding fiber section. Frequency shift W and temporal shift T are affected by amplifier noise and change in a random fashion. If we add fluctuations at each amplifier as random kicks at the location of each amplifier, W and T vary along the fiber link according to the equations

$$\frac{\mathrm{d}W}{\mathrm{d}z} = \sum_i \delta W_i\delta(z - z_i), \tag{6}$$

$$\frac{\mathrm{d}T}{\mathrm{d}z} = \beta_2 W + \sum_i \delta T_i\delta(z - z_i), \tag{7}$$

where δW_i and δT_i are the random frequency and time kicks imparted by noise at the ith amplifier. These kicks depend on the amplifier-noise strength and on various pulse parameters such as width and chirp of the pulse. The GH jitter can be calculated by solution of Eqs. (6) and (7).

3. FREQUENCY AND TIME KICKS

Before proceeding with the jitter calculation, we need to know the statistical properties of the random frequency and time kicks inside each amplifier. Let δU be the amount by which amplifier noise changes pulse amplitude U. At each amplifier, δU is a random function of time. Furthermore, the changes imposed by different amplifiers are independent. These properties are quantified by the equations

$$\langle\delta U_i(t_i)\delta U_j(t_j)\rangle = 0, \tag{8}$$

$$\langle\delta U_i^*(t_i)\delta U_j(t_j)\rangle = S_i\delta_{ij}(t_i - t_j), \tag{9}$$

where $\langle\ \rangle$ denotes an ensemble average. Source term $S_i = n_{\mathrm{sp}}h\nu(G_i - 1)$, where n_{sp} is the spontaneous-emission factor[6] h is the Planck constant, ν is the carrier frequency of the pulse, and G_i is the amplification provided by the ith amplifier. Physically, S_i represents the spectral density of spontaneous-emission noise.

To quantify the statistical properties of the frequency and time kicks we use Eqs. (3) and (4) to determine the kicks and Eqs. (8) and (9) to evaluate their correlations. Because the changes in pulse amplitude at the various amplifiers are independent, so also are the frequency and time kicks. At any amplifier, the frequency and time kicks have the properties (the subscript i is not shown explicitly for simplicity of notation)

$$\langle\delta W^2\rangle = (2S/E^2)\int_{-\infty}^{\infty}|V_t|^2\mathrm{d}t, \tag{10}$$

$$\langle\delta W\delta T\rangle = (iS/2E^2)\int_{-\infty}^{\infty}(t - T)(V^*V_t - VV_t^*)\mathrm{d}t, \tag{11}$$

$$\langle\delta T^2\rangle = (2S/E^2)\int_{-\infty}^{\infty}(t - T)^2|V|^2\mathrm{d}t, \tag{12}$$

where $V = U\exp(iWt)$. Equations (10)–(12) were derived by Grigoryan *et al.*,[7] who used the numerical solution of the nonlinear Schrödinger equation in the absence

of noise to find U and calculate the variances and the cross correlation of δW and δT.

We use a different approach that permits us to evaluate these quantities approximately in an analytic form. More specifically, we employ the Gaussian-shape ansatz, that is used commonly in a variational analysis of DM systems and has been found through numerical simulations to be reasonable.[10–14] In this approach each pulse is approximated by a chirped Gaussian pulse of the form

$$U = a \exp[i\phi - iW(t - T) - (1 + ic)(t - T)^2/2\tau^2], \tag{13}$$

where amplitude a, phase ϕ, frequency W, time delay T, chirp c, and width τ are functions of z. By substituting Eq. (13) into Eqs. (10)–(12) we find that

$$\langle \delta W^2 \rangle = (S/E)[(1 + c^2)/\tau^2], \tag{14}$$

$$\langle \delta W \delta T \rangle = (S/E)c, \tag{15}$$

$$\langle \delta T^2 \rangle = (S/E)\tau^2. \tag{16}$$

As expected, variances of frequency and time kicks, and their correlation, are directly proportional to noise strength S but are inversely proportional to pulse energy E. This inverse dependence on pulse energy is in agreement with the Gordon–Haus result[1] when it is written in a nonnormalized form. In fact, the Gordon–Haus result can be obtained from the moment method if the fiber is assumed to have uniform dispersion and the pulse shape is assumed to be unchirped, with a sech profile. It should be stressed that, although the moment method is applicable for pulses of arbitrary shapes, Eq. (13) assumes Gaussian-shaped pulses. For this reason, Eqs. (14)–(16) can also be obtained by use of a variational approach based on the Gaussian-shape ansatz.

4. GROWTH OF FREQUENCY AND TIME SHIFTS

In this section we calculate how the frequency and time kicks imparted at each amplifier accumulate as the pulse traverses the entire fiber link. To simplify the calculation we use the minimum pulse width τ_m along the link (i.e., the width of the pulse at the transmitter before it is chirped) for normalization purposes. We introduce $\bar{W} = W\tau_m$ and $\bar{T} = T/\tau_m$ as normalized frequency and time shifts but ignore the overbar for notational simplicity. As a result, W and T are dimensionless quantities in what follows.

To consider the most general case, we allow for the possibility that more than one amplifier may be used within each stage (map period). Consider a DM system with n_s stages, each of which has n_a amplifiers. Henceforth we use subscript i to denote a stage number and subscript j to denote an amplifier number within a stage. By integrating Eqs. (6) and (7) over the fiber section between the $(j - 1)$st and the jth amplifier within the ith stage and averaging the results, we find that

$$\langle W^2 \rangle_j = \langle W^2 \rangle_{j-1} + \langle \delta W_j^2 \rangle, \tag{17}$$

$$\langle WT \rangle_j = \langle WT \rangle_{j-1} + d_j \langle W^2 \rangle_{j-1} + \langle \delta W_j \delta T_j \rangle, \tag{18}$$

$$\langle T^2 \rangle_j = \langle T^2 \rangle_{j-1} + 2d_j \langle WT \rangle_{j-1} + d_j^2 \langle W^2 \rangle_{j-1} + \langle \delta T_j^2 \rangle, \tag{19}$$

where

$$d_j = \frac{1}{\tau_m^2} \int_{z_{j-1}}^{z_j} \beta_2(z)\mathrm{d}z \tag{20}$$

is related to the net dispersion in the fiber section between the amplifiers $j - 1$ and j. With the exception of d_j, all quantities in Eqs. (17)–(19) depend implicitly on i.

We apply Eqs. (17)–(19) repeatedly to model pulse propagation over the entire ith stage. The result is given by

$$\langle W^2 \rangle_i = \langle W^2 \rangle_{i-1} + A_i, \tag{21}$$

$$\langle WT \rangle_i = \langle WT \rangle_{i-1} + d_s \langle W^2 \rangle_{i-1} + B_i, \tag{22}$$

$$\langle T^2 \rangle_i = \langle T^2 \rangle_{i-1} + 2d_s \langle WT \rangle_{i-1} + d_s^2 \langle W^2 \rangle_{i-1} + C_i, \tag{23}$$

where $d_s = \Sigma_{j=1}^{n_a} d_j$ is the net dispersion of each stage and

$$A_i = \sum_{j=1}^{n_a} \langle \delta W_j^2 \rangle, \tag{24}$$

$$B_i = \sum_{j=1}^{n_a} \langle \delta W_j \delta T_j \rangle + \sum_{j=1}^{n_a - 1} \langle \delta W_j^2 \rangle \left(\sum_{k=j+1}^{n_a} d_k \right), \tag{25}$$

$$C_i = \sum_{j=1}^{n_a} \langle \delta T_j^2 \rangle + 2 \sum_{j=1}^{n_a - 1} \langle \delta W_j \delta T_j \rangle \left(\sum_{k=j+1}^{n_a} d_k \right) + \sum_{j=1}^{n_a - 1} \langle \delta W_j^2 \rangle \left(\sum_{k=j+1}^{n_a} d_k \right)^2. \tag{26}$$

Coefficients A_i and C_i are the noise-induced changes in the frequency and time variances that accumulate over stage i, and B_i is the noise-induced change in the correlation. Whereas A_i depends only on the frequency kicks, B_i depends on the correlation kicks and the frequency kicks (modified by dispersion) and C_i depends on the time kicks, the correlation kicks, and the frequency kicks (modified by dispersion).

Equation (23) can be used for calculating the GH timing jitter over the ith stage. One obtains the total timing jitter by adding the contributions of n_s stages. However, this step requires knowledge of the coefficients in Eqs. (24)–(26). The jitter calculation is simplified considerably for DM solitons, which propagate from stage to stage in a periodic fashion. For this reason we consider the soliton case first. The nonsoliton case in which pulses propagate from section to section in a linear but aperiodic fashion is considered afterward.

5. PERIODIC PROPAGATION

In this section we apply our general formalism to DM soliton systems. Soliton systems are designed such that the pulse parameters recover their initial values at the end of each stage of length equal to the map period.[15–18] The periodic nature of pulse propagation simplifies the summations in Eqs. (21)–(23) considerably because A_i, B_i,

and C_i become independent of i. For this reason we drop the subscript i from these quantities. We use the variational analysis of DM systems[12–14] to find the three pulse parameters E, τ, and c at the beginning of the first stage. We assume that the initial chirp is generated by propagation of the pulse through a fiber (called precompensation fiber) of length L_p and dispersion β_{2p}. For such a light-wave system it is possible to solve Eqs. (21)–(23) iteratively for an arbitrary number of stages. The result is given by

$$\langle W^2\rangle_{n_s} = An_s, \tag{27}$$

$$\langle WT\rangle_{n_s} = Bn_s + Ad_s(n_s - 1)/2, \tag{28}$$

$$\langle T^2\rangle_{n_s} = Cn_s + Bd_sn_s(n_s - 1) + Ad_s^2n_s(n_s - 1)(2n_s - 1)/6, \tag{29}$$

where A, B, and C include the sum over the number of amplifiers per stage, as indicated in Eqs. (24)–(26). Equation (29) is our main result in this section. Our approach provides an analytic expression for the timing jitter that is valid even when multiple amplifiers are used within each stage. This equation also applies to the case of dense DM in which multiple map periods are used between two amplifiers.[8]

The values of the coefficients A, B, and C in Eq. (29) depend on the dispersion map and the gain distribution, which determine the pulse energy and the prechirp. To demonstrate the most interesting features as simply as possible, we focus on a 10-Gbit/s system, using two specific dispersion maps with a map period L_m of ~80 km (typical value in practice) and consider how the jitter is affected when a second amplifier is placed within each stage. One map consists of a 76-km anomalous-GVD section of dispersion-shifted fiber [D = 4 ps/(km-nm), α=0.2 dB/km, $A_{\rm eff}$ = 55 μm^2], followed by a 3.6-km section of dispersion-compensating fiber [D = −80 ps/(km-nm), α=0.4 dB/km, $A_{\rm eff}$ = 55 μm^2], resulting in an average dispersion of $\bar{D}$ = 0.2 ps/(km/nm). For the 30-ps (full width $T_{\rm FW}$ at half-maximum) unchirped pulses used for numerics, the map strength, defined as

$$S = |D_1L_1 - D_2L_2|/T_{\rm FW}^2, \tag{30}$$

has a relatively low value of S = 0.62 for this map. An amplifier is placed at the end of each DM stage of length L_m = 79.6 km. The spectral density of noise is calculated from n_{sp} = 1.3 (noise figure of ~4.1 dB for the lumped amplifier). The solid curve in Fig. 1 shows the timing jitter at the end of each amplifier as a function of transmission distance for τ_m = 18.02 ps ($T_{\rm FW}$ = 30 ps), $n_{\rm sp}$ = 1.3, and $h\nu$ = 0.8 eV. The input chirp is c_0 = 0.25 and the input peak power is P_0 = 2.74 mW for solitons propagating in such a light-wave system.

To see how the jitter is affected by a second amplifier placed in each DM stage, we optimize the location of the second amplifier such that pulse breathing is minimized. For the map under consideration this occurs when the amplifier is placed at a transmission distance of 35 km in the dispersion-shifted fiber section of the map. The dotted curve in Figure 1 shows that the GH jitter is reduced considerably when two amplifiers are used within each DM stage. We can understand this result by noting that the gain of each amplifier is lower, resulting in a lower value of spectral density S. In Fig. 1 the jitter is reduced by a factor of ~2 when two amplifiers are used.

The second map is designed with standard fiber and consists of a 66-km anomalous-GVD section of standard-telecommunication fiber [D = 16 ps/(km-nm), α=0.2 dB/km, $A_{\rm eff}$ = 55 μm^2], followed by a 13-km section of dispersion-compensating fiber [D = −80 ps/(km-nm), α=0.4 dB/km, $A_{\rm eff}$ = 55 μm^2], resulting in an average dispersion of approximately $\bar{D}$ = 0.2 ps/(km-nm). From Eq. (30), the map strength with $T_{\rm FW}$ = 30 ps is given by S = 2.33, indicating considerable breathing of pulse width in each map period. An amplifier is placed at the end of each DM stage of length L_m = 79 km. The solid curve in Fig. 2 shows the timing jitter at the end of each amplifier as a function of transmission distance for solitons of the same width used in Fig. 1 to ensure a fair comparison. The input chirp is c_0 = 0.765 and the input peak power is P_0 = 4.86 mW for solitons propagating in such a light-wave system. The dashed curve in Fig. 2 shows how jitter is affected when a second amplifier is placed within each DM stage at a transmission distance of 24 km (location optimized to minimize pulse breathing). For this location of the amplifier, P_0=0.944 mW, c_0 = 2.05, and the chirp at the intermediate amplifier is 0.534.

A comparison of Figs. 1 and 2 shows several interesting features. Timing jitter is smaller for the map made with the standard fiber when one amplifier is used in each stage. This is a consequence of the higher pulse peak powers needed for a map with larger strengths. The resultant larger values of pulse energy E reduce fluctuations as indicated in Eqs. (10)–(12). The second amplifier may increase or decrease the jitter, depending on transmission distance L. For distances up to 2400 km the GH jitter is greater when two amplifiers are used in each stage. For longer distances the second amplifier reduces

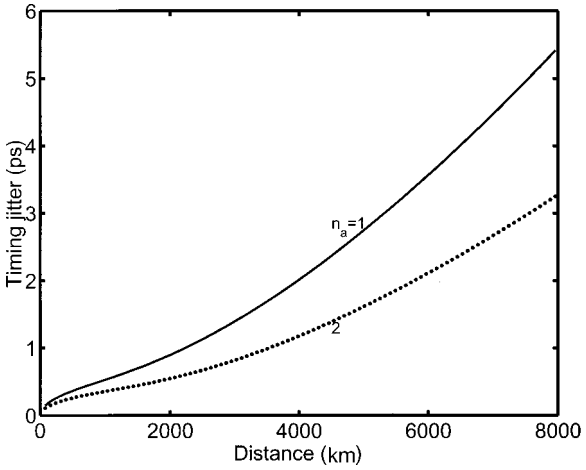

Fig. 1. Timing jitter for a 10-Gbit/s soliton DM system as a function of transmission distance. A single amplifier is placed at the end of each 79-km map period (solid curve), whereas a second amplifier is present at a transmission distance of 35 km for the dashed curve. The map has a strength of 0.62 and an average dispersion of 0.2 ps/(km-nm).

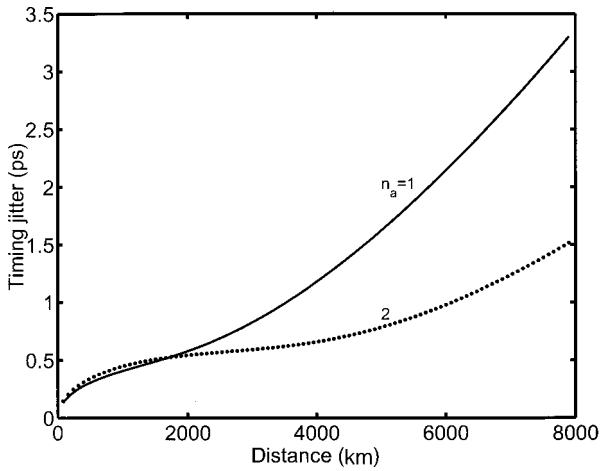

Fig. 2. Same as Fig. 1, except that here the map consists of 66 km of standard fiber followed by 13 km of dispersion-compensating fiber, resulting in a map strength of 2.33 and an average dispersion of 0.2 ps/(km-nm). The second amplifier is placed at a transmission distance of 24 km.

the jitter by a large amount (as much as a factor of 4 in Fig. 2). The reason behind this somewhat surprising result is related to the contribution of the B term in Eq. (29). The second term in Eq. (25) depends on the GVD accumulated up to the location of the amplifier. For an amplifier located at the end of each map period, $|d_k|$ in Eq. (25) is relatively small, but it can be quite large for the second amplifier located within the map. As a result, the B term contribution becomes large at moderate distances even though this term grows as L^2 while the A term grows as L^3. This discussion indicates that the use of multiple amplifiers in each map period can be beneficial for light-wave systems designed with standard fibers but that the amplifier locations should be chosen judiciously.

To study the multiamplifier case analytically and find the extent of jitter reduction, we consider the GH timing jitter in long-haul light-wave systems for which n_s is so large that the dominant contribution to timing jitter comes from the A term in Eq. (29), which exhibits a cubic dependence on n_s. As discussed above, this limit may require more than 100 amplifiers, depending on the map design. In the limit $n_s \gg 1$, the dominant A term becomes

$$\langle T^2 \rangle_{n_s} \approx A n_s (n_s d_s)^2/3. \tag{31}$$

Coefficient A is obtained from Eqs. (14) and (24). If we use the relation $(1 + c_0^2)/\tau_0^2 \approx 1/\tau_m^2$, where τ_m is the minimum pulse width within each map period (that is also equal to the width of the pulse at the transmitter before it is launched into the precompensation fiber), we can rewrite relation (31) in physical units as

$$\langle T^2 \rangle_{n_s} \approx \frac{n_{\rm sp} h \nu \bar{\beta}_2^2 L^3}{3 l_s \tau_m^2} \sum_{j=1}^{n_a} \frac{G_j - 1}{E_j}, \tag{32}$$

where l_s is the length of a single stage and $L = n_s l_s$ is the length of the entire DM system. The quantities E_j and G_j represent the pulse energy at the end of the jth amplifier with gain G_j.

Relation (32) generalizes the previously derived expression for timing jitter[8] to the case in which multiple amplifiers are used within each map period. Many light-wave systems are designed with only one amplifier per stage. In that case the last factor reduces to $[\exp(\alpha l_s) - 1]/E_0$, where E_0 is the energy of pulses launched at the input end and the two kinds of fiber within the map are assumed to have the same value of loss parameter α (it is assumed to be different in numerical simulations, as is also the case in practice). With several identical amplifiers per stage such that they have the same gain and are spaced apart by l_s/n_a, $G_j = \exp(\alpha l_s/n_a) = G_t^{1/n_a}$, where $G_t = \exp(\alpha l_s)$ is the total gain of the all amplifiers in each stage of length l_s. The pulse energy at the output of each amplifier is also the same because each amplifier is designed to recover the input pulse energy. We can thus set $E_j = E_0$ in relation (32). The change in timing jitter with the use of multiple amplifiers is then given by a reduction factor defined as

$$f_r(n_a) = \frac{\langle T^2 \rangle_{n_a}}{\langle T^2 \rangle_{n_a=1}} = n_a \frac{G_t^{1/n_a} - 1}{G_t - 1}. \tag{33}$$

Figure 3 shows the reduction factor as a function of n_a for several values of stage length l_s (map period). Although there is a limit to how large n_a can be in practice, the use of several amplifiers reduces timing jitter in the same way that it reduces amplifier noise.[19] The reduction factor is relatively small when the stage length is only 25 km but can exceed 5 for a 75-km map. Notice also that almost the entire reduction occurs when a second or third amplifier is placed. For a 75-km map, the second amplifier reduces the jitter by a factor of 3. This result is consistent with that shown in Fig. 1 when the second amplifier is roughly in the middle of the map. In the case of Fig. 2, the second amplifier is not in the middle, and Eq. (33) does not apply. Nevertheless, jitter is seen to be reduced by approximately a factor of 3.

The limit in which n_a tends to infinity corresponds to the case of uniformly distributed amplification. Our analysis shows that timing jitter is reduced when distributed amplification is used in place of one lumped amplifier per stage, and the reduction factor is given by

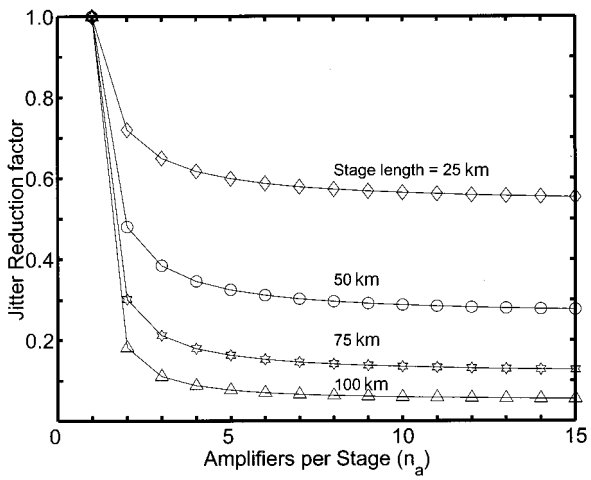

Fig. 3. Reduction in timing jitter when several amplifiers are placed at equal distances in each map period.

$$\frac{\langle T^2\rangle_{\text{distrib}}}{\langle T^2\rangle_{\text{lumped}}} = \frac{\alpha l_s}{\exp(\alpha l_s) - 1} = \frac{\ln G_t}{G_t - 1}, \tag{34}$$

where G_t is the total gain of the single lumped amplifier. As a simple example, for an 80-km map period, $G_t = 40$ if we assume a total loss of 16 dB over $l_s = 80$ km. Timing jitter should be reduced by a factor of 10.6 according to Eq. (34). However, this result is based on the assumption that input pulse parameters remain unchanged in the two cases. In practice, the periodicity condition requires lower pulse energies in the case of distributed amplification. Inasmuch as frequency noise variance scales inversely with E in Eq. (14), the reduction in timing jitter in practice is expected to be considerably smaller than that predicted by Eq. (34).

6. EFFECT OF POSTCOMPENSATION

In this section we consider the effect of postcompensation of residual dispersion $n_s d_s$ on the timing jitter. A postcompensation fiber of length L_f with dispersion β_{2f} is placed after the last amplifier such that the total dispersion of the entire fiber link becomes small (even zero). We can calculate the effects of a postcompensation fiber on the frequency and time shifts, and their correlation, by omitting the noise terms in Eqs. (21)–(23) and replacing $i - 1$ with n_s, i with f, and d_s with $d_f = \beta_{2f} L_f / {\tau_m}^2$. Focusing again on the dominant A term, which varies as ${n_s}^3$, and introducing $y = -d_f/(n_s d_s)$, where y represents the fraction of postcompensation, we find the final jitter at the end of the postcompensation fiber:

$$\langle T^2\rangle_f \approx A n_s (n_s d_s)^2 (y^2 - y + 1/3). \tag{35}$$

The minimum value occurs for $y = 0.5$, and the jitter variance is reduced by a factor of 4 for this minimum value. The same conclusion was reached in an earlier study in which constant-dispersion fibers were used.[20] Our analysis shows that postcompensation is also useful for DM soliton systems.

To study how postcompensation affects timing jitter, we consider the 10-Gbit/s soliton systems with the dispersion map used for Fig. 2 [$\bar{D} = -0.2$ ps/(km-nm), $S = 2.33$]. Figure 4 shows changes in timing jitter for several values of y when a single amplifier per map period is used. In the absence of postcompensation ($y = 0$), jitter becomes quite large with increasing distance (the dotted curve in Fig. 4). Even a small value of postcompensation reduces jitter considerably. The three most noteworthy properties of the single-amplifier system are that (i) jitter can be reduced but cannot be eliminated through postcompensation, (ii) jitter can be minimized with an optimum length of postcompensation fiber ($y = 0.5$), and (iii) 100% postcompensation makes the situation worse than when there is no compensation. We have also shown what happens when $y = -0.5$ to emphasize that even an increase in the net dispersion is better for distances below 2500 km rather than full compensation ($y = 1$). This is so because the B term in Eq. (29) also contributes significantly to the timing jitter for moderate distances, whereas relation (35) is based on the dominant A term.

One can reduce the timing jitter whether d_s is positive or negative. However, if d_s has the same sign as the GVD of the first fiber in each stage (and hence the sign opposite the GVD of the prechirp fiber), the GVDs of the prechirp and postcompensation fibers will have the same sign, and the pulses will broaden monotonically in the postcompensation fiber. This broadening may reduce the eye opening. Consequently, postcompensation is most useful when the average GVD has the sign opposite that of the GVD of the first fiber in each stage, and the reduction in timing jitter coincides with the narrowing of the pulses in the postcompensation fiber.

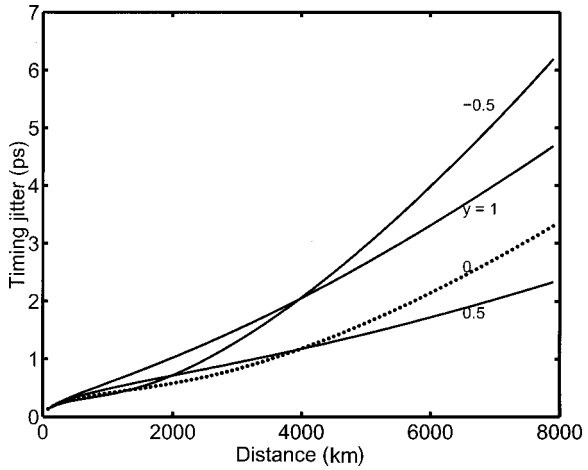

Fig. 4. Effect of postcompensation on timing jitter of a 10-Gbit/s DM soliton system for the dispersion map used in Fig. 2 (map strength, $S = 2.33$). Jitter is plotted as a function of transmission distance for four values of y that represent the fraction of postcompensation.

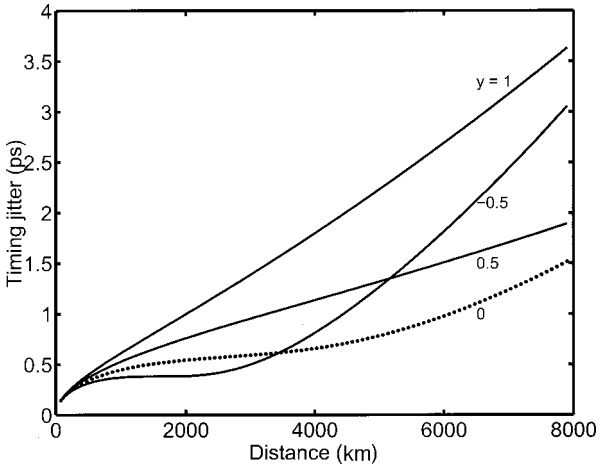

Fig. 5. Same as Fig. 4, except that a second amplifier is placed at a transmission distance of 24 km.

An interesting question is whether postcompensation remains an effective technique for reducing timing jitter even when several amplifiers are used in each map period. Figure 5 shows the jitter under conditions identical to those of Fig. 4, except that here a second amplifier is placed at a transmission distance of 24 km (location optimized to reduce the extent of pulse breathing). The optimum value of y is now given by $y_{\text{opt}} = 0.5 + B/(A n_s d_s)$. It depends on the ratio B/A and varies from -0.5 to 0.5 as the as the distance increases above 10,000 km. Indeed, in Fig. 4 negative values of y, which

increase the net dispersion, produce the lowest value of timing jitter for distances up to 5000 km. The reason for this is related to the contribution of the B term in Eq. (29), which scales as ${n_s}^2$. As discussed above, this behavior is caused by the B term in Eq. (20), which is proportional to the chirp and scales as ${n_s}^2$. The presence of the second amplifier causes the chirp to be large at the location of the first amplifier. It appears that the contribution of the B term can be canceled under some conditions by use of negative values of postcompensation parameter y. These results suggest that the role of postcompensation requires a careful analysis when multiple amplifiers are used in each map period.

7. APERIODIC PROPAGATION

In this section we focus on a CRZ light-wave system in which input pulses are prechirped and then propagated along the DM link in a quasi-linear fashion without the necessity for periodicity; i.e., pulse width and chirp are not intended to recover their input values after each amplifier. A postcompensation fiber is still used to reduce the average dispersion to close to zero. We investigate how timing jitter evolves in such a quasi-linear aperiodic system. As before, both time and frequencies are normalized with τ_m for scaling.

For (low-power) CRZ systems,[21–24] the dependences of chirp and width on distance are well approximated by analytical solutions of the linear Schrödinger equation.[4] In fact, the combination $(1 + c^2)/\tau^2$ remains constant because it is related to the pulse spectral width, which remains unchanged in a linear system. Consequently, when the average dispersion is nonzero, the chirp and the width have different values at every amplifier in every stage. The solution of Eqs. (21)–(23) can be written in terms of width τ_m of the unchirped width at the transmitter. Let c_{ij} be the chirp at the jth amplifier in the ith stage. Then the linear propagation of a pulse through the aperiodic DM system shows that the chirp accumulates as

$$c_{ij} = c_0 + \left[(i - 1)d_s + \sum_{k=1}^{j} d_k\right], \tag{36}$$

where $c_0 = d_p = \beta_{2p}L_p/{\tau_m}^2$ is the (initial) chirp at $z = 0$. Here β_{2p} is the dispersion parameter of the fiber of length L_p used for pulse prechirping.

In the linear regime the frequency kicks do not depend on the pulse shape. They do depend on the pulse energy and the amplifier gain, both of which evolve periodically. It follows from Eqs. (14) and (24) that

$$A_i = \sum_{j=1}^{n_a} \langle \delta {W_j}^2 \rangle = S_j/E_j \tag{37}$$

is independent of i. In what follows, we use A in place of A_i to use this feature explicitly. In contrast, B_i and C_i do depend on stage index i. The correlation kicks depend on the chirp, which depends on i and j. By substituting Eq. (36) into Eq. (25) we obtain

$$B_i = A(c_0 + id_s). \tag{38}$$

The time kicks depend on ${\tau^2}/{\tau_m}^2 = 1 + c^2$, which depends on i and j. By substituting Eq. (36) into Eq. (26) we find that

$$C_i = A[1 + (c_0 + id_s)^2]. \tag{39}$$

Although the solution of Eqs. (21)–(23) requires more algebra for variable coefficients than for constant coefficients, the algebra is straightforward. The variances and the cross correlation of W and T are found to be given by the relatively simple expressions

$$\langle W^2 \rangle_{n_s} = An_s, \tag{40}$$

$$\langle WT \rangle_{n_s} = An_s(n_s d_s + d_p), \tag{41}$$

$$\langle T^2 \rangle_{n_s} = An_s[1 + (n_s d_s + d_p)^2]. \tag{42}$$

As can be seen, the three moments depend on the simple combination $n_s d_s + d_p$, which is the total dispersion along the link. To calculate the effects of a postcompensation fiber on frequency and time shifts, and their correlation, we omit the noise terms in Eqs. (21)–(23) and replace $i - 1$ with n_s, i with f, and d_s with d_f. The final result is

$$\langle W^2 \rangle_{n_s} = An_s, \tag{43}$$

$$\langle WT \rangle_{n_s} = An_s(n_s d_s + d_p + d_f), \tag{44}$$

$$\langle T^2 \rangle_{n_s} = An_s[1 + (n_s d_s + d_p + d_f)^2]. \tag{45}$$

The three moments depend only on the total (precompensated and postcompensated) dispersion. Equations (43)–(45) are multiple-amplifier generalizations of the single-amplifier equations in Ref. 8. The timing jitter expression in Eq. (45) is quite simple. We focus on it in Section 8.

8. EFFECTS OF PRECOMPENSATION AND POSTCOMPENSATION

In the absence of precompression or postcompensation, the timing jitter of a quasi-linear DM system with $d_s \neq 0$ varies as

$$\langle T^2 \rangle_{n_s} \approx An_s(n_s d_s)^2. \tag{46}$$

Comparison with the soliton case shows that the GH jitter is larger for the linear DM system by a factor of 3 if we assume the same pulse energy in both cases. However, validating the quasi-linear approximation requires that pulse energy E be lower, making the GH jitter larger by more than a factor of 10 for low-energy pulses. It can be reduced significantly by use of two or more amplifiers per map period. Figure 6 shows, as an example, the GH jitter for a CRZ system designed with the same dispersion map used for Fig. 2 (66 km of standard fiber with 13 km of dispersion-compensated fiber). To ensure the quasi-linear nature of pulse propagation, we take the peak power of each pulse to be only 10% of the peak power needed in the case of DM solitons. At a distance of 8000 km, jitter exceeds 18 ps when only one amplifier is used every 79 km. This value of jitter is so large that a 10-Gbit/s quasi-linear system would be inoperable. How-

ever, the use of a second amplifier reduces the jitter to 7 ps, a value that is acceptable for 10-Gbit/s systems.

A comparison of Figs. 2 and 6 shows that the timing jitter is larger for a CRZ system than for a DM soliton system. The reason for large jitter in Fig. 6 is related to the residual dispersion of 0.2 ps/(km-nm) for each map period. One can reduce the final variance of the timing jitter to An_s by setting $d_p + d_f = -n_s d_s$, a condition that corresponds to complete dispersion compensation. This behavior is confirmed in Fig. 6, which shows that the jitter is reduced to 3 ps when postcompensation reduces the average GVD to zero for the entire link. This value should be compared with the $y = 1$ curve in Fig. 4, where the effect of complete postcompensation on solitons is shown. The GH jitter under such conditions is less for a linear CRZ system than for DM solitons.

Although the final timing jitter does not depend on the ratio of precompensation to postcompensation, the timing jitter within the system does. In a purely linear CRZ system, it does not matter how d_p and d_f are chosen as long as $d_p + d_f = -n_s d_s$. However, most practical CRZ systems suffer from nonlinear effects to some extent. An important nonlinear effect is related to pulse-to-pulse interactions. One might try to minimize the timing jitter within the entire system to minimize the effects of pulse-to-pulse interactions. At the end of stage i the timing jitter is given by Eq. (42), with n_s replaced by i. It is convenient to rewrite the right-hand side of Eq. (42) as $An_s(n_s d_s)^2 F(z, x)$, where

$$F(z, x) = z[\epsilon + (z - x)^2]. \tag{47}$$

$z = i/n_s$ is the fractional distance, $x = -d_p/(n_s d_s)$ is the fractional precompensation, and $\epsilon = 1/(n_s d_s)^2$. In most cases, $\epsilon \ll 1$, and we can determine the optimal compensation ratio perturbatively. The analysis is facilitated by the idealization that z is a continuous variable. When $x = 0$, F is a monotonically increasing function of z. When $0 < x \leqslant 1$, F has a local maximum within the system. This local maximum is attained when

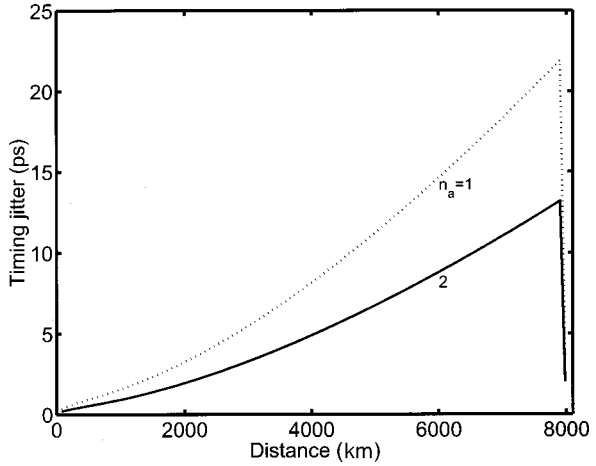

Fig. 6. Timing jitter for a 10-Gbit/s quasi-linear CRZ system as a function of transmission distance for the same map used for Fig. 2. The second amplifier, placed at a transmission distance of 24 km, reduces the jitter by a factor of ~3 (dotted curve).

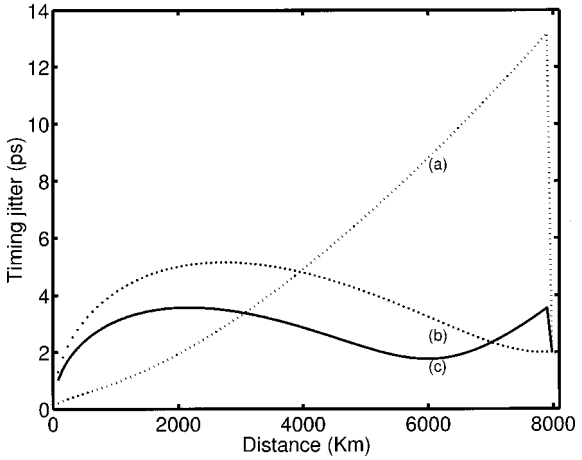

Fig. 7. Effects of precompensation and postcompensation on timing jitter of a 10-Gbit/s CRZ system for the same dispersion map used in Fig. 2: (a) No precompensation and complete postcompensation; (b) complete precompensation and no postcompensation; (c) 77% precompensation and 23% postcompensation.

$$z_m \approx x/3 + \epsilon/2x. \tag{48}$$

The interior timing jitter is governed by the function $F[z_m(x), x]$, which is an increasing function of x. In contrast, the boundary timing jitter (at the end of each stage) is governed by $F(1, x)$, which is a decreasing function of x. The maximum value of jitter in each stage is the larger of the two timing jitters. It attains its minimum when $F[z_m(x), x] = F(1, x)$. This condition is satisfied when

$$x_m \approx 3/4 + \epsilon. \tag{49}$$

This simple result predicts that the jitter along the entire link can be minimized when ~75% of the link dispersion is compensated for at the transmitter, with the remaining 25% compensated for after the last amplifier.

To verify this prediction numerically, in Fig. 7 we plot timing jitter as a function of n_s for two amplifiers per map period and the same dispersion map that was used in Fig. 6. The peak power of each pulse is again only 10% of the peak power needed in the case of DM solitons. Figure 7 shows that for a specific choice $x_m \approx 3/4$ of precompensation and postcompensation, the jitter is indeed minimized along the entire CRZ system at the location of amplifiers.

The preceding analysis describes how one can minimize the timing jitter within the system at the ends of various stages. According to Eq. (7), the timing jitter oscillates between the amplifiers within each stage. For systems in which pulse-to-pulse interactions facilitated by timing jitter cause severe problems, intrastage oscillations in timing jitter should also be taken into account, in a manner similar to that described in Section 7.

9. SUMMARY

In this paper we have presented an analytic theory of timing jitter in DM light-wave systems based on the moment method and on the assumption of a chirped Gaussian pulse. Our expression of the timing jitter can be used in the case of dense DM systems achieved by use of multiple

map periods between two neighboring amplifiers. It also applies in the opposite case in which more than one amplifier is used within each map period.

We have applied the general formalism to a soliton DM system and found a simple analytic expression for the timing jitter at the ends of such systems. We used this result to study the effect of a second amplifier within each map period on the timing jitter. Depending on the dispersion map's details and the transmission distance, the total jitter may increase or decrease when two amplifiers per map period are used. In the case of a dispersion map composed with fibers with high local dispersion (large map strength), the use of a second amplifier can reduce the total jitter considerably for long-haul systems, provided that the second amplifier is placed at a location that reduces the extent of pulse breathing.

We have investigated the effect of postcompensation of the total accumulated dispersion on timing jitter of soliton systems. Our results indicate that postcompensation can be beneficial, provided that its magnitude is optimized properly. More specifically, postcompensation of residual dispersion by 50% reduces the jitter by a factor of 2 at long distances when a single amplifier is used for each map period. However, jitter actually increases if the residual dispersion is eliminated completely by use of a postcompensation fiber. When there are two or more amplifiers within each map period the situation becomes complex, to the extent that an increase in the average dispersion may reduce the jitter for moderate distances.

We also applied our analytic theory to a low-power CRZ system designed such that a prechirped pulse propagates through the dispersion map without recovering its initial values at the end of each map period. We were able to obtain a relatively simple analytic expression for the timing jitter in such systems, even including the effects of both precompensation and postcompensation. In general, 100% compensation of the total dispersion is essential for realizing jitter values comparable with those obtained for DM solitons. One may ask what fraction of the dispersion should be precompensated. We used our analytic formula to explore the optimum values of precompensation and postcompensation and found that the timing jitter can be minimized all along the fiber link when 75% of the total dispersion is compensated for at the transmitter while the remaining 25% is compensated for at the receiver end for large distances.

ACKNOWLEDGMENTS

We thank T. I. Lakoba, D. Q. Chowdhury, and S. P. Burtsev for helpful discussions. This research is supported in part by the National Science Foundation under grants ECS-9903580 and DMS-0073923.

G. P. Agrawal's e-mail address is gpa@optics.rochester.edu.

*Present address: Bell Laboratories, Lucent Technologies, 791 Holmdel-Keyport Road, Holmdel, New Jersey 07733.

REFERENCES

1. J. P. Gordon and H. A. Haus, "Random walk of coherently amplified solitons in optical fiber transmission," Opt. Lett. **11**, 665–667 (1986).
2. A. Hasegawa and Y. Kodama, *Solitons in Optical Communications* (Clarendon, Oxford, 1995).
3. R. J. Essiambre and G. P. Agrawal, "Timing jitter of ultrashort solitons in high-speed communication systems: general formulation and application to dispersion-decreasing fibers," J. Opt. Soc. Am. B **14**, 314–322 (1997).
4. G. P. Agrawal, *Fiber-Optic Communication Systems*, 2nd ed. (Wiley, New York, 1997), Chap. 10.
5. E. Iannone, F. Matera, A. Mecozzi, and M. Settembre, *Nonlinear Optical Communication Networks* (Wiley, New York, 1998), Chap. 5.
6. G. P. Agrawal, *Applications of Nonlinear Fiber Optics* (Academic, San Diego, Calif., 2001).
7. V. S. Grigoryan, C. R. Menyuk, and R. M. Mu, "Calculation of timing and amplitude jitter in dispersion-managed optical fiber communications using linearization," J. Lightwave Technol. **17**, 1347–1356 (1999).
8. J. Santhanam, C. J. McKinstrie, T. I. Lakoba, and G. P. Agrawal, "Effects of precompensation and postcompensation on timing jitter in dispersion-managed systems," Opt. Lett. **26**, 1131–1133 (2001).
9. S. N. Vlasov, V. A. Petrishchev, and V. I. Talanov, "Averaged description of wave beams in linear and nonlinear media (the method of moments)," Radiophys. Quantum Electron. **14**, 1062–1070 (1971).
10. I. R. Gabitov, E. G. Shapiro, and S. K. Turitsyn, "Optical pulse dynamics in fiber links with dispersion compensation," Opt. Commun. **134**, 317–329 (1997).
11. V. S. Grigoryan, T. Yu, E. A. Golovchenko, C. R. Menyuk, and A. N. Pilipetskii, "Dispersion-managed soliton dynamics," Opt. Lett. **23**, 1609–1611 (1997).
12. V. S. Grigoryan and C. R. Menyuk, "Dispersion-managed solitons at normal average dispersion," Opt. Lett. **23**, 609–611 (1998).
13. A. Berntson, N. J. Doran, W. Forysiak, and J. H. B. Nijhof, "Power dependence of dispersion-managed solitons for anomalous, zero, and normal path-average dispersion," Opt. Lett. **23**, 900–902 (1998).
14. T. I. Lakoba, J. Yang, D. J. Kaup, and B. A. Malomed, "Conditions for stationary pulse propagation in the strong dispersion management regime," Opt. Commun. **149**, 366–375 (1998).
15. L. F. Mollenauer, J. P. Gordon, and P. V. Mamyshev, in *Optical Fiber Telecommunications*, I. P. Kaminow and T. L. Koch, eds. (Academic, San Diego, Calif., 1997), Vol. 3A, Chap. 12; see also references therein.
16. E. Yamada, H. Kubota, T. Yamamoto, A. Sahara, and M. Nakazawa, "10 Gbit/s, 10600km, dispersion-allocated soliton transmission using conventional 1.3 μm single mode fibres," Electron. Lett. **33**, 602–603 (1997).
17. I. S. Penketh, P. Harper, S. B. Alleston, A. M. Niculae, I. Bennion and N. J. Doran, "10-Gbit/s dispersion-managed soliton transmission over 16,500 km in standard fiber by reduction of soliton interactions," Opt. Lett. **24**, 802–804 (1999).
18. L. F. Mollenauer, P. V. Mamyshev, J. Gripp, M. J. Neubelt, N. Mamysheva, L. Gruener-Nielsen, and T. Veng, "Demonstration of massive wavelength-division multiplexing over transoceanic distances by use of dispersion-managed solitons," Opt. Lett. **25**, 704–706 (2000).
19. A. Yariv, "Signal-to-noise considerations in fiber links with periodic or distributed optical amplification," Opt. Lett. **15**, 1064–1066 (1990).
20. W. Forysiak, K. J. Blow, and N. J. Doran, "Reduction of Gordon–Haus jitter by posttransmission dispersion compensation," Electron. Lett. **29**, 1225–1226 (1993).
21. A. D. Ellis and D. M. Spirit, "Unrepeatered transmission over 80 km standard fibre at 40 Gbit/s," Electron. Lett. **30**, 72–74 (1994).
22. R. Ludwig, W. Pieper, H. G. Weber, D. Breuer, K.

Petermann, F. Kueppers, and A. Mattheus, "Unrepeatered 40 Gbit/s RZ single-channel transmission over 150km of standard single-mode fibre at 1.55 μm," Electron. Lett. **33**, 76–77 (1997).
23. D. Breuer, H. J. Ehrke, F. Kueppers, R. Ludwig, K. Petermanm, H. G. Weber, and K. Weich, "Unrepeated 40-Gb/s RZ single-channel transmission at 1.55 μm using various fiber types," Photonics Technol. Lett. **10**, 822–824 (1998).
24. E. A. Golovchenko, A. N. Pilipetskii, N. S. Bergano, C. R. Davidson, F. I. Khatri, R. M. Kimball, and V. J. Mazurczyk, "Modeling of transoceanic fiber-optic WDM communication systems," IEEE J. Sel. Top. Quantum Electron. **6**, 337–347 (2000).